

# Self Supervised Networks for Learning Latent Space Representations of Human Body Scans and Motions

Emmanuel Hartman<sup>1,2</sup>      Martin Bauer<sup>1</sup>  
Nicolas Charon<sup>2</sup>  
Florida State University<sup>1</sup> University of Houston<sup>2</sup>

November 7, 2024

## Abstract

This paper introduces self-supervised neural network models to tackle several fundamental problems in the field of 3D human body analysis and processing. First, we propose VariShaPE (Varifold Shape Parameter Estimator), a novel architecture for the retrieval of latent space representations of body shapes and poses. This network offers a fast and robust method to estimate the embedding of arbitrary unregistered meshes into the latent space. Second, we complement the estimation of latent codes with MoGeN (Motion Geometry Network) a framework that learns the geometry on the latent space itself. This is achieved by lifting the body pose parameter space into a higher dimensional Euclidean space in which body motion mini-sequences from a training set of 4D data can be approximated by simple linear interpolation. Using the SMPL latent space representation we illustrate how the combination of these network models, once trained, can be used to perform a variety of tasks with very limited computational cost. This includes operations such as motion interpolation, extrapolation and transfer as well as random shape and pose generation.

## 1 Introduction

### 1.1 Motivation

The examination of human body shapes holds significant importance in various fields such as computer vision, graphics, and virtual reality. The key deliverables in this areas include:

1. Fast algorithms for **clustering and classification** of (large scale) data of unregistered human body scans;
2. Efficient computational frameworks for **accurate motion transfer, motion interpolation and motion extrapolation**;
3. **Generative modelling** via empirical distributions learned from (large scale) unregistered human body scan data bases.

Numerous studies [2, 16, 29, 19, 24] have focused on addressing these challenging computational tasks by parameterizing the space of human body shapes using low-dimensional latent space models. However, several difficulties persist with these latent space parameterizations.

One key challenge consists in the non-uniqueness of the raw shape data, i.e., the same human body shape can be represented by infinitely many different mesh representation. In the continuous (smooth) setting this non-uniqueness is encoded by defining two shapes to be the same if they

only differ by a reparametrization. The analogue in the discrete setting is to consider two human body scans (represented as simplicial complexes) to be the same if they only differ by a remeshing operation. This non-uniqueness makes the task of retrieving latent code representations from unregistered data significantly more challenging. In the quest for faithful latent space representation of the space of human body shapes it is thus paramount to develop mesh invariant latent space representations from raw body scans with minimal mesh preprocessing and computational demands.

A second key challenge consists of the fact that the linear geometry of a given latent space representation will not accurately describe the non-linear nature of human body movements, which brings up the challenging task of accurately capturing the geometry of human motions within latent spaces and thereby obtaining a faithful computational framework based on these latent space representations.

## 1.2 Contributions

Towards these ends, we propose two self-supervised deep learning models which can be used in conjunction to address these demands:

1. First, we introduce **VariShaPE** (Varifold Shape Parameter Estimator), a self-supervised neural network model for real-time mesh invariant latent space encoding of human body scans;
2. Second, we derive **MoGeN** (Motion Geometry Network), a framework for learning the geometry of human body motion latent spaces from 4D-data.

We note that, as demonstrated in Section 4, these two models can be used in conjunction to obtain efficient (real time) and accurate algorithms for operations such as motion transfer, generative modelling and 4D-interpolation. Next we describe the benefits of the two methods, as compared to state-of-the-art algorithms, in more details.

### Benefits of VariShaPE and Comparison to State-of-the-art Methods:

Finding low-dimensional parametric representation for the statistical analysis of human shapes is an active research area [2, 16, 29], that dates back to the groundbreaking work on 3D Morphable Models for faces by Blanz et al. [4]. In the particular case of modelling for whole body scans, common approaches include skeleton based models in combination with physically motivated transformation models. Among those, one of the most widely used approaches, is the SMPL latent space [19], which is learned from thousands of 3D body scans; see also [26, 24] for recent extensions that further enhance this model by adding eg. articulated hands and face expressions.

Our first contribution, VariShaPE, deals with the challenging task of estimating such latent space representations given raw data, i.e., to retrieve the best latent parameter to fit a given unregistered scan of a human body. Standard methods for this retrieval task are usually optimization based and often require manual intervention in order to lead to satisfactory results [19]; this includes spectral based methods such as the functional map framework [25], minimizing the Hausdorff or Chamfer distance [9, 13], or methods based on Riemannian geometry and elastic shape analysis [15]. In contrast to these methods our model employs a self-supervised network approach making use of concepts of geometric measure theory [18], which allows us to incorporate shape invariances directly in the network architecture and thereby significantly boost the performance of the corresponding algorithms.

A further key benefit of the proposed VariShaPE model is that it can be trained on (applied to, resp.) raw scans without any additional mesh preprocessing. This is precisely due to the

aforementioned geometric measure theory inspired architecture, which is specifically designed to ensure complete mesh invariance, i.e., our model will produce (approximately) the same latent code representations of scans that represent the same human body invariant to the mesh structure or scanning noise which appears in real data. An additional benefit of our framework is the fast training time as compared to other network-based approaches in human shape analysis. This again stems from our use of geometrically motivated constructions in the network, which allows us to encode the invariances of the data directly in the corresponding architecture. Thereby we are able to significantly reduce the amount of trainable parameters and thus require an order of magnitudes lower amount of training time as compared to previous approaches such as LIMP [8], ARAPReg [17], or 3D-Coded [13]. Finally we present results that show our latent code retrieval framework is competitive with the state of the art 3D-Coded [13] method for shape registration while requiring orders of magnitude less computational time, c.f Table 1 in Section 3.1. Additionally we provide experiments to highlight our models superior robustness to mesh resampling, c.f Table 2 in Section 3.1.

### **Benefits of MoGeN and Comparison to State-of-the-art Methods:**

Once data (eg. human body scans) is embedded in a linear (Euclidean) latent space, one directly obtains a corresponding framework for statistical analysis: operations such as interpolation and extrapolation can be simply defined by performing these operations in the linear latent space. In the context of human body scans, this raises the issue of whether the linear geometry of the latent space accurately describes the complex movements and deformations appearing in such data, see also [21, 20, 30] for a discussion on this matter in the context of latent space interpolation for general machine learning applications.

Indeed, the performance of such a naive approach is rather limited in the context of large movements of human bodies. To address these issues multiple (physically motivated) deformation energy losses have been introduced in the training phase, thereby altering the corresponding latent space: this includes geodesic distances [8], the As-Rigid-As-Possible (ARAP) energy [17, 22], or volumetric constraints [3]. See also [31, 10] for an approach using manifold regularization of learned pose spaces. These geometric quantities, however, significantly increase the total training costs of those approaches. More importantly, they are still based on user-defined assumption to model the movement of human shapes. Our work differs in two different aspects from these approaches: first we keep the latent space unchanged, but instead equip it with a different non-linear geometry. Secondly, we do not make any assumptions on the physics behind the deformations of human body motions, but instead learn them in a purely data-driven approach using 4D training data. In our experiments we argue that this data driven approach leads to a significantly improved performance in terms of interpolation and extrapolation accuracy. A further key benefit of this methodology is that it allows us to capture more complex motions of human bodies, including those which reach the "boundary" of feasible human motions.

### **Future work and Choice of Latent Space Model:**

In summary, we have proposed in this paper new self-supervised models for learning not only latent space representations of human body shape and pose but also the underlying geometry of the latent space itself. The latter one is achieved through the introduction of an additional lifted space in which observed body pose motions get unfolded to straight paths. We have further shown how these two frameworks can be used to perform common tasks such as motion interpolation, extrapolation and transfer, and to estimate generative models in the space of human body pose and shape.

In our experimental section, we demonstrate the capabilities of our models using data from the DFAUST dataset and by employing the SMPL model (A Skinned Multi-Person Linear body model) [19] as the corresponding latent space representation. We want to emphasize, that our framework is not tied in any way to this particular choice, but could be directly applied to any other existing latent space representation for human bodies, such as SMPL-X [26], STAR [24], BLISS [23] or the elastic shape analysis basis representation used in [15, 28]. While we aim to extend our framework in future work to these latent spaces, we decided to focus in the experiments of this present paper on the SMPL representation, due to its convenient implementation in PyTorch and its wide use in the human body shape community. In one of our ablation studies, cf. Appendix A, we demonstrate a similar performance using the elastic shape analysis basis setting as an alternative latent space representation; in future work we plan to explore the use of some of the recent SMPL extensions, such as the above mentioned STAR [24].

## 2 Methods Section

In this section we will introduce the main methodological contribution of the present work. We start by introducing the space of triangular meshes  $\mathcal{S}$ .

A mesh with  $m_v$  vertices and  $m_f$  faces is described by an ordered set of vertices  $\mathcal{V} = \{v_i\}_{i=1}^{m_v} \subseteq \mathbb{R}^3$  and an ordered set of faces described by the indices of the vertices of the face  $\mathcal{F} = \{f_j\}_{j=1}^{m_f} \subseteq (1, 2, \dots, m_v) \times (1, 2, \dots, m_v) \times (1, 2, \dots, m_v)$ . The space of meshes is then defined as

$$\mathcal{S} := \left\{ \left( \{v_i\}_{i=1}^{m_v}, \{f_j\}_{j=1}^{m_f} \right) \text{ s.t. } m_v \in \mathbb{N} \text{ and } m_f \in \mathbb{N} \right\}.$$

Note, that the elements of  $\mathcal{S}$  can differ both in the mesh face connectivity or even in the total number of elements (edges and faces, resp.).

**Remark 1** (Non-uniqueness of mesh representations). *It is important to note, that the representation of a human body as an element of  $\mathcal{S}$ , i.e., as a triangulated mesh, comes with several ambiguities: many meshes can represent the same human scan and thus one has to compare these representations up to shape preserving transformations. These shape preserving transformations are given by translation, rotation and (most importantly) general remeshing operations such as subdivision algorithms.*

In the exploration of human body surfaces, a prevalent strategy for tackling the dimension reduction problem involves adopting a latent space model. Such a model is essentially a mapping  $F$  from a latent space  $\mathcal{L}^F \subset \mathbb{R}^n$  to the space of triangulated surfaces  $\mathcal{S}$ . Various construction methods, such as data-driven basis construction or skinned skeletal models, can be employed to build such latent spaces, see [19, 26, 24, 23, 28] and the references therein. The first focus of this paper is to solve the inverse problem associated with a fixed latent space model, i.e, for an arbitrary mesh  $q$  and a given latent space model  $F : \mathcal{L}^F \rightarrow \mathcal{S}$  we aim to find  $v \in \mathcal{L}^F$  such that  $F(v)$  and  $q$  represent the same shape. We will refer to this as the *latent code retrieval problem*.

To deal with the aforementioned non-uniqueness in the mesh representation of a human body shape, we will start by introducing a concept from geometric measure theory, which will allow us to define a fixed-dimension, mesh invariant feature vector representation, which we can then used as the input to train a fully connected neural network,  $\Psi_\theta$ , parameterized by weights  $\theta = \{\theta_i\}$ , mapping this feature vector representation into the latent space  $\mathcal{L}^F$ .

## 2.1 The Varifold Gradient as a Shape Descriptor

Many works in the field of human body analysis, including the aforementioned references [19, 9, 13], have relied on the well-known Chamfer or variants of the Hausdorff distance to define loss functions for surface reconstruction or estimation of latent representations. However, these typically result in loss functions that are not differentiable at every point. Alternatives, which arguably lead to better regularity and stability properties, can be obtained via representations of surfaces in measure spaces equipped with kernel metrics [7] (also known as maximum mean discrepancy in statistics [11]), among which the varifold framework has recently seen several applications to the field [1, 27, 15]. In the present work, we will leverage varifolds for two specific purposes:

1. to obtain a reliable notion of surface distance to evaluate and benchmark our proposed algorithms and, more importantly,
2. to obtain a mesh invariant feature representation for the proposed VariShaPE method for solving the latent code retrieval problem.

Let us briefly recap the primary features of the varifold framework for surface meshes, referring to [18, 7] for more detailed presentations:

**Definition 1** (Varifold distance). *Given two triangulated surfaces  $q, q' \in \mathcal{S}$  denote by  $\{f_1, \dots, f_m\}$  and  $\{f'_1, \dots, f'_{m'}\}$  the respective set of non-degenerate triangular faces in  $q$  and  $q'$ . The (squared) varifold distance is then computed by examining all possible pairs of faces in the following way:*

$$\begin{aligned}
 d_{\text{Var}}(q, q')^2 = & \sum_{i=1}^m \sum_{j=1}^m \rho(|c_{f_i} - c_{f_j}|) \frac{(n_{f_i} \cdot n_{f_j})^2}{|n_{f_i}| |n_{f_j}|} + \sum_{i=1}^{m'} \sum_{j=1}^{m'} \rho(|c_{f'_i} - c_{f'_j}|) \frac{(n_{f'_i} \cdot n_{f'_j})^2}{|n_{f'_i}| |n_{f'_j}|} \\
 & - 2 \sum_{i=1}^m \sum_{j=1}^{m'} \rho(|c_{f_i} - c_{f'_j}|) \frac{(n_{f_i} \cdot n_{f'_j})^2}{|n_{f_i}| |n_{f'_j}|}
 \end{aligned} \tag{1}$$

where for a face  $f$  (of  $q$  or  $q'$ ),  $c_f$  denotes its barycenter,  $n_f$  is the normal vector of length equal to the area of  $f$  and where  $\rho$  is a given kernel function. For notational purposes we denote the squared distance from a fixed shape  $q$  by  $D_q(q') := d_{\text{Var}}(q, q')^2$ .

Note, that the above definition does not assume that the surfaces  $q$  and  $q'$  are registered, i.e., their number of vertices and triangles may differ and no prior correspondences are known.

**Remark 2** (Choice of kernel function). *In this work we choose the kernel function  $\rho$  to be a centered Gaussian which variance can be interpreted as the spatial scale of the metric. In particular, we choose  $\rho(|c - c'|) = e^{-\frac{|c-c'|^2}{\sigma^2}}$  with  $\sigma = 0.025$ . Note that many other choices of kernels on the face centers and normals are also possible, c.f. [18].*

Furthermore, we point out that the squared distance in (1) is differentiable with respect to the vertex positions of  $q$  and  $q'$  provided the kernel function  $\rho$  is smooth enough. The gradients can be easily computed either explicitly from (1) or via automatic differentiation, with high numerical efficiency on a GPU due to the very parallelizable nature of this computation. This allows us to introduce the gradient of the varifold distance, which we will later use as a fixed dimension shape descriptor:

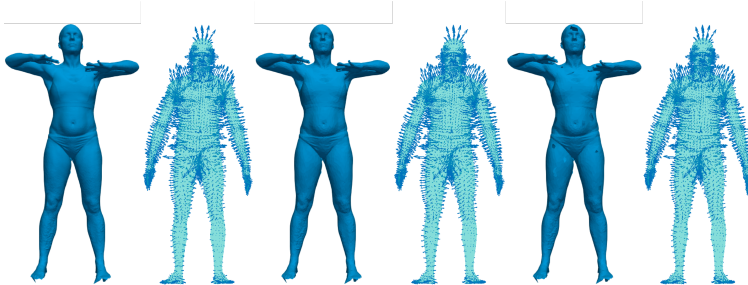


Figure 1: Plots of the varifold distance gradient field from the neutral pose template surface paired with three different target surfaces  $q'$ . These correspond to the same shape at full resolution (237k faces, left), lower resolution (20k faces, middle) and with added topological noise (right). One can see that the resulting field remains remarkably unaffected by those changes.

**Definition 2** (VariGrad Shape Representation). *Given a fixed template mesh  $\bar{q} \in \mathcal{S}$  with  $M$  vertices we define*

$$\text{VariGrad} : \begin{cases} \mathcal{S} & \rightarrow \mathbb{R}^{3M} \text{ given by} \\ q & \mapsto \nabla D_q(\bar{q} + (\cdot))(0). \end{cases}$$

For our purposes, the main advantage of the VariGrad representation is given by the following two properties:

1.  $\text{VariGrad}(q)$  is a vector field on  $\bar{q}$  and thus has fixed dimension  $3M$  independently of the dimension of the input mesh  $q$ . Intuitively, it encodes the positioning of  $q$  with respect to  $\bar{q}$ ; a formal analogy can be drawn with the gradient of a squared Riemannian distance that corresponds to the logarithm map of the manifold.
2. Due to the properties of varifold metrics it is essentially invariant to resampling or mesh changes in the surface represented by  $q$  as well as certain amount of imaging noise, which is showcased in the example of Figure 1.

Thus it can be leveraged as an effective feature representation for latent space neural network learning models, as has been recently shown in the context of curves and shape graphs, see [14].

## 2.2 Latent Code Retrieval: Mesh Invariant Feature Vectors and the Varifold Shape Parameter Estimation (VariShaPE) Framework

We are now ready to introduce the proposed model for solving the latent code retrieval problem. Inspired by the recent work on curves and shape graphs [14] the underlying idea is to combine the mesh invariant VariGrad representation with a fully connected neural network,  $\Psi_\theta$ , which is trained to learn the mapping from this fixed dimension feature vector space into the given latent space model  $F : \mathbb{R}^n \supset \mathcal{L}^F \rightarrow \mathcal{S}$ .

The drawback of this approach in the context of human body surfaces is that the template requires a large number of vertices to be sufficiently expressive, thereby producing a high dimensional feature vector representation and thus a higher computational complexity for training. To circumvent this difficulty we will construct a feature space utilizing a second reduced dimension latent space model  $G : \mathbb{R}^m \supset \mathcal{L}^G \rightarrow \mathcal{S}$  and define a shape descriptor based on this model as follows:

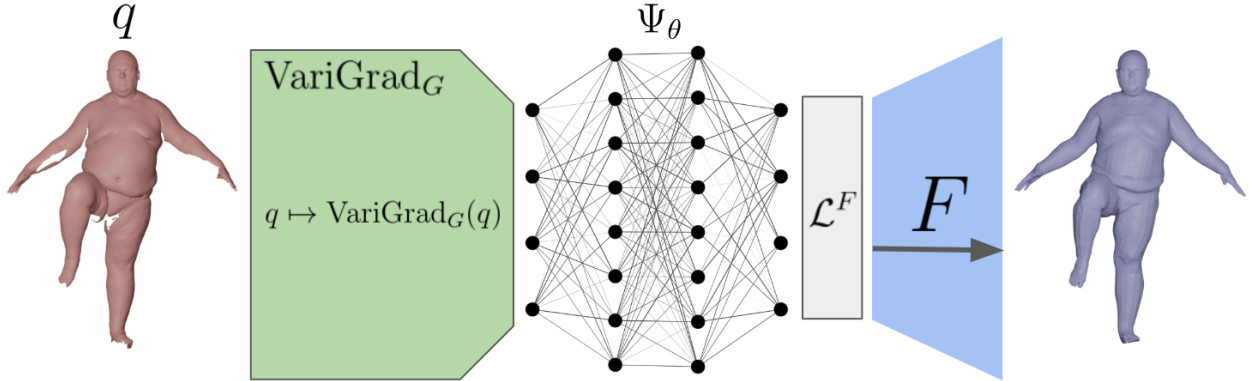


Figure 2: Illustration of the proposed VariShaPE framework: The framework utilizes two non-trainable latent space models: The first,  $G$ , is utilized to construct feature vectors from unregistered meshes using the VariGrad operator defined above. The second,  $F$ , parameterizes the space of human bodies. Given an input mesh  $q$  with arbitrary mesh structure, we compute the VariGrad shape descriptor with respect to the parameters of the model  $G$ ,  $\text{VariGrad}_G(q)$ . These parameterization invariant features are passed through a trainable MLP with parameters  $\theta$  to predict a latent space representation of  $q$  with respect to the target latent space model  $F$ . As one can see in the example presented in this figure, our framework is robust to imaging noise, i.e., holes and small missing parts stemming eg. from imaging noise are not significantly influencing the reconstruction procedure.

**Definition 3** (Latent space constrained VariGrad Shape Representation). *For a given latent space model  $G : \mathbb{R}^m \supset \mathcal{L}^G \rightarrow \mathcal{S}$  we define the VariGrad shape descriptor as*

$$\text{VariGrad}_G : \begin{cases} \mathcal{S} & \rightarrow \mathcal{L}^G \subset \mathbb{R}^m \text{ given by} \\ q & \mapsto \nabla(D_q \circ G)(\vec{0}). \end{cases}$$

Note that the unrestricted VariGrad of Definition 2 corresponds to the particular case in which  $G(u) = \bar{q} + u$ . The advantage of introducing a more general latent space model  $G$  lies in the fact that we only calculate the gradient w.r.t. the variables of a lower-dimensional latent space. Thus the latent space constrained VariGrad operator produces shape descriptors with a potentially (order of magnitudes) lower dimension than that of Definition 2 while still remaining insensitive to mesh resampling. It is important to note, that this additional latent model  $G$  can be chosen independently of the targeted latent space representation  $F$ ; it is merely a computational tool and (beyond computational accuracy) it is not influencing the final latent code retrieval. This is supported by our experiments, see Section 3 and the ablation study in the supplementary material, in which we choose different latent models for  $F$  and  $G$  and justify our particular choices.

The latent code retrieval algorithm, which we propose can then be summarized as follows

- for an arbitrary mesh representing a human body,  $q$ , we consider the latent space constrained VariGrad shape descriptor (see Definition 3) for a frozen latent space model  $G : \mathbb{R}^m \rightarrow \mathcal{S}$  to define an  $m$ -dimensional mesh invariant descriptor of  $q$ .
- These representations are then used as inputs to an MLP  $\Psi_\theta$ , which is trained to learn the desired latent code representation  $v \in \mathcal{L}^F$ .

- We train the model so that  $F(v)$  and  $q$  represent the same shape, i.e., we consider a Loss function of the form

$$\text{Loss}(F(v)) = D_q(F(v)), \quad (2)$$

where  $\text{dist}$  is an appropriate similarity measure on the space of triangulated surfaces.

A schematic of this framework is presented in Figure 2. It remains to specify the loss function  $\text{Loss}$ , for which there are several natural choices: if the available training data has the same mesh structure as the outputs of the model  $F$  (with consistent point correspondences) we can train the model to simply minimize the mean vertex error (MVE) between  $F(v)$  and  $q$ , i.e.,

$$\text{Loss}^{\text{MVE}}(F(v)) := \frac{1}{k} \sum_{i=1}^k \|F(v)_i - q_i\|^2. \quad (3)$$

Alternatively if such training data is not available, then the Chamfer distance and Varifold distance (as defined in (1)) both offer differentiable loss functions for training data without point to point correspondences to the outputs of  $F$ . For the experiments presented in this paper, we train with a subset of the DFAUST dataset (c.f Section 3) which falls under the former category, and thus we present results of the model trained with the mean vertex error as the loss function of the model. An ablation study for these other choices of loss functions is given in Section B.

**Remark 3.** *In recent years, several other frameworks for sampling invariant feature vector representations of geometric data have been proposed. In the context of point clouds, PointNet [6] and Dynamic Graph Convolutional Neural Networks (DGCNN) [32], propose frameworks for constructing global features with fixed dimension representing this data. As we will see in the experiments section, our approach leads to a significantly improved performance for dealing with the resampling (remeshing, resp.) problem as compared to the PointNet and DGCNN architectures.*

### 2.3 Learning the Latent Space Geometry

In this section, we specifically focus on the situation where our latent space representation can be decomposed into a Pose Parameter Space (i.e., those parameters that govern the motion/pose of the object) and a Shape Parameter Space (i.e., those parameters that govern the identity/body type of the object). This is a typical feature in the construction of human body latent spaces as is the case, for instance, with the SMPL model. As there is no ground truth for the deformation of one human body into another human body, we will equip the Shape Parameter Space simply with the linear Euclidean geometry. The goal of this section is to learn the geometry of the Pose Parameter Space, so that human motions from 4D data are “geodesics” with respect to this geometry. Namely, our goal is to learn a “geometry” such that the following two operations correspond to natural human motions:

1. **Interpolation** (the “geodesic” boundary value problem), which corresponds to finding the path (deformation) between two different latent codes .
2. **Extrapolation** (the “geodesic” initial value problem), which corresponds to finding the trajectory given one latent code and an initial deformation direction.

To achieve this goal, we train a model comprised of two maps  $f : \mathcal{L}^F \rightarrow \mathbb{R}^N$  and  $\pi : \mathbb{R}^N \rightarrow \mathcal{L}^F$ . Note, that the dimension of the auxiliary space  $\mathbb{R}^N$  is usually chosen to be significantly larger than the dimension of the target latent space  $\mathcal{L}^F$ , i.e., in our experiments we picked  $N = 4n$ .



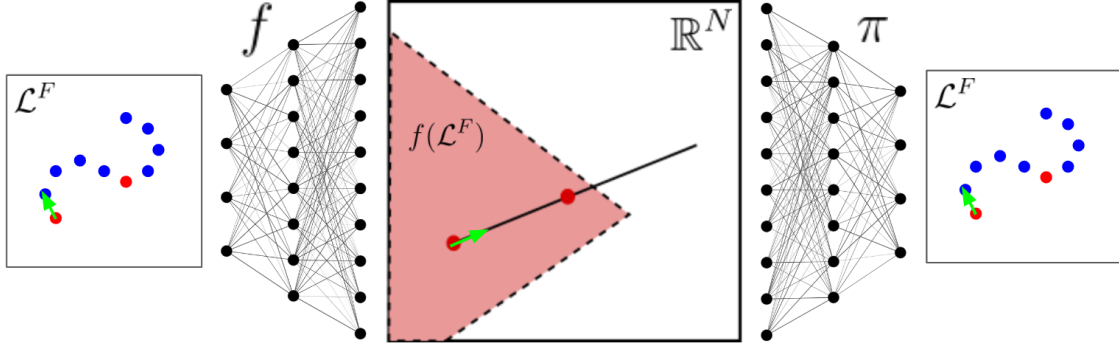


Figure 3: Illustration of the proposed MoGeN framework: Given two points in latent space (a point and a deformation direction, resp.), the network  $f$  maps them into a high dimensional, lifted latent space, where interpolation (extrapolation, resp.) follow the standard linear paths. Subsequently, they are projected back to the original latent space using the network  $\pi$ , which allows the user to map them into the space of surfaces using the decoder  $F$ . The networks  $f$  and  $\pi$  are trained according to the loss function defined in Equation (4). In the above depiction, the boundary points are plotted in red, whereas the initial deformation direction is plotted in green.

Given a 4D sequence  $\alpha_1, \dots, \alpha_T$  of latent codes representing a human motion, we then define the loss function

$$\text{Loss}^{\text{MoGen}}(\alpha_1, \dots, \alpha_T) = \frac{1}{2T} \sum_{i=1}^T \underbrace{\text{MSE}(\hat{\alpha}_i, \alpha_i)}_{\text{Interpolation Loss}} + \underbrace{\text{MSE}(\alpha'_i, \alpha_i)}_{\text{Extrapolation Loss}} \quad (4)$$

where MSE denotes the mean squared error and where

$$\hat{\alpha}_i = \pi \left( f(\alpha_0) + i \frac{f(\alpha_T) - f(\alpha_0)}{T-1} \right) \quad \text{and} \quad \alpha'_i = \pi(f(\alpha_0) + i(f(\alpha_1) - f(\alpha_0))).$$

Here the first term is called *Interpolation Loss* as it measures the deviation of the linear interpolation based on the first and last time point to the given data to the given human body mini sequence. In contrast, the second term is called the *Extrapolation Loss* as it measures the deviation of the linear extrapolation based on the first two time points to the given data. It is important to note, that our training ensures  $\pi \circ f \approx \text{Id}_{\mathcal{L}}$ , but that we will not have  $f \circ \pi = \text{Id}_{\mathbb{R}^N}$  in general. The extrapolation loss ensures in addition that  $\pi$  learns to map elements of  $\mathbb{R}^N$  which are not in  $f(\mathcal{L})$  consistently with neighboring points in  $f(\mathcal{L})$ . This ensures that our framework learns appropriate behavior near the boundary of feasible human motions. We will also demonstrate the advantage of this feature in the experimental section, cf. Figures 6 and 7. For a schematic description of the general latent space geometry procedure we refer to Figure 3.

### 3 Experimental Results

In this section we will perform several experiments to demonstrate the accuracy of the proposed network models and compare them to the state-of-the-art algorithms in the area. We start by describing the computational infrastructure and datasets used in our experiments.

### Computational Infrastructure:

All experiments were performed on a standard home PC with a Intel 3.2 GHz CPU and a GeForce GTX 2070 1620 MHz GPU.

### Datasets:

We train our models on the Dynamic FAUST (DFAUST) dataset [5]. This database contains high resolution 4D scans captured at 60 Hz of 10 individuals performing 14 in-place motions. These involve scanning errors and occlusions which lead to topological noise in the data. These 4D sequences are registered using image texture information and a body motion model creating sequences of meshes with fixed point to point correspondences. Furthermore the meshes in these registered sequences share point to point correspondences with outputs of many latent space models such as [19, 26, 28]. We then split this data so that 80 percent of the sequences are used in training and 20 percent are used in testing. Additionally, for the selected testing sequences we also utilize the corresponding raw scans to evaluate the performance of the proposed VariShaPE model on meshes with topological noise and scanning errors and without fixed point to point correspondence. To train and validate the MoGeN model, we use the VariShaPE architecture to extract latent code representations of the training and testing sequences and subsequently extract mini-sequences of pose parameters from these sequences.

#### 3.0.1 Evaluation methods:

In our experiments, we will evaluate the results using different similarity measures: first we calculate the mean vertex distance, which is only available for registered meshes. Secondly, we evaluate the methods using the varifold metric introduced in Section 2.1. In order to avoid any bias, as our method is partially based on this distance measure, we will also use the Chamfer distance [9, 13] as an additional measure of quality. Note, that only the mean vertex distance and the Chamfer distance have an interpretation in physical units (i.e., in millimeters), but that for the varifold kernel distance such an interpretation is not available.

### 3.1 VariShaPE: Mapping Registered and Unregistered Scans to SMPL

	Registered				Unregistered			
	Chamfer Search	ARAPReg VAE [17]	3D Coded [13]	Ours	Chamfer Search	ARAPReg VAE [17]	3D Coded [13]	Ours
Mean Vertex Dist. (mm)	6.3	5.1	2.5	<b>2.1</b>	NA	NA	NA	NA
Varifold Error	0.047	0.038	<b>0.024</b>	0.035	0.048	NA	<b>0.035</b>	<b>0.036</b>
Chamfer Error (mm)	3.1	2.9	<b>2.3</b>	2.5	5.7	NA	3.2	<b>2.9</b>
Time of $10^3$ Recon.	6339.4s	2.1s	4403.1s	<b>0.8s</b>	9311.6s	NA	7012.3s	<b>1.0s</b>
Training	<b>None</b>	2w	12hrs	<b>8hrs</b>	<b>None</b>	NA	12hrs	<b>8hrs</b>

Table 1: Reconstruction Results: We compute the mean vertex distance for the unseen registered testing data and mean Chamfer and varifold errors for all of the meshes in the registered and unregistered testing sets.

### Experimental setup:

In our first set of experiments we aim to demonstrate the capability of the VariShaPE model to learn a map from unregistered meshes into the latent space  $\mathcal{L}^F$  of the SMPL model. Therefore we choose  $G$  as the affine decoder described in [15] and  $F$  to be the base, gender-neutral SMPL

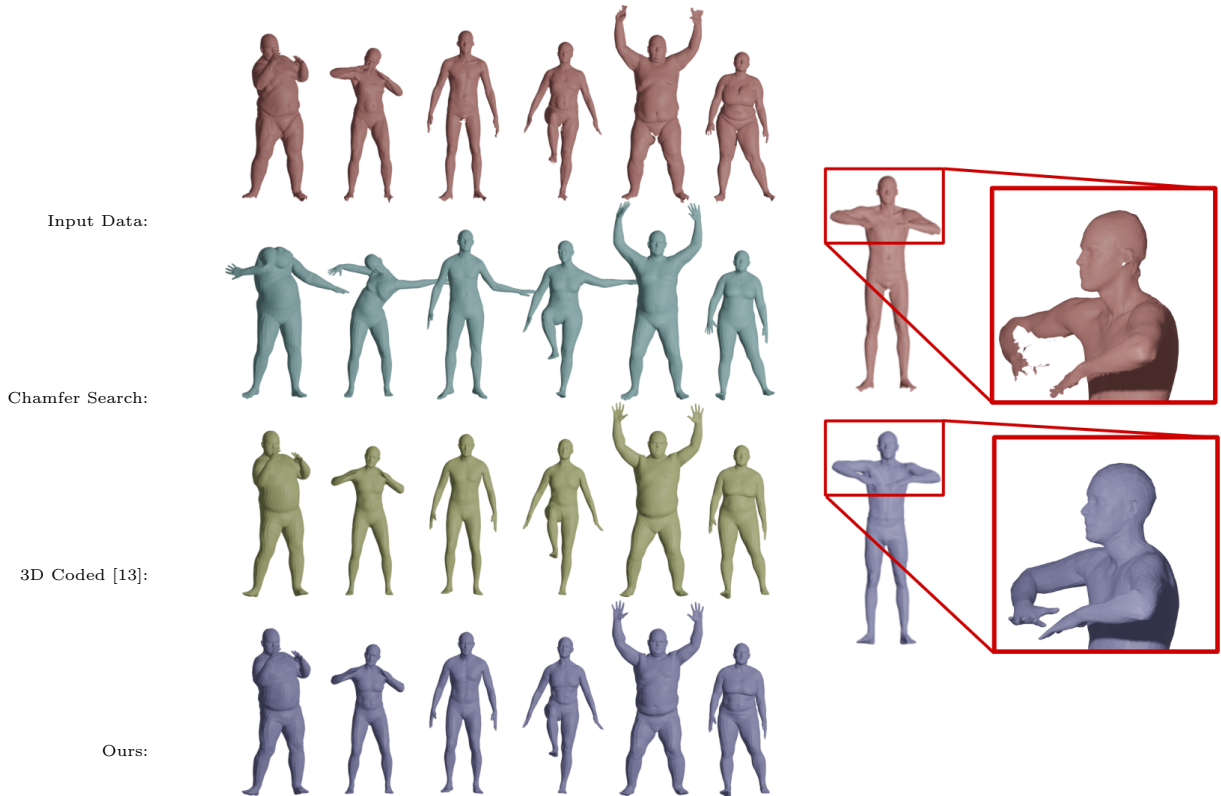


Figure 4: Qualitative Comparison of mesh retrieval methods for unregistered data: We display 6 raw scans of human meshes, reconstructions produced by Chamfer search, reconstructions produced by the 3D-Coded model [13], and reconstructions produced via our model. One can clearly see the superior performance of our model and 3D-Coded as compared to Chamfer search. Investigating the results of 3D-Coded in more detail one can see that the output of this model fails to accurately capture fine (textural) details of the human body shapes, such as clothes or the muscles structure on the core. In contrast our model performs significantly better in regards with these fine details. Additionally, we highlight our model’s robustness to noise and scanning errors, as can be seen in the highlighted box at the very right.

model [19]. This leads to latent space dimensions of  $m = 170$  and  $n = 375$ . In the appendix we present an ablation study for different choices of latent space models for both  $F$  and  $G$  and show that these lead to a comparable performance. The network  $\Psi_\theta$  is then constructed as a sequence of fully connected layers separated by ReLU activation functions with a total of  $3 \times 10^6$  trainable parameters. We train the model with registered meshes from the DFAUST dataset, i.e., we train the model to minimize the mean square error between the vertices of the training meshes and the reconstruction of the learned parameters of the model. An ablation study on the choice of Loss function is shown in appendix B, where one can see that this simple choice of loss function strikes a good balance between computational complexity and quality of the results.

### Comparison methods:

For comparison of our latent code retrieval capabilities we use three other state-of-the-art methods: first we simply run an optimization over the latent space using an L-BFGS optimizer minimizing the Chamfer distance between the target mesh and the reconstruction of the latent code. This method works for both registered and unregistered meshes as the Chamfer distance does not rely on point to point correspondences and we will refer to it as Chamfer search. Second, we compare the resulting reconstructions to the variational auto-encoder network of [17]. This approach is trained with registered data to construct a latent space representation of human bodies which is regularized by an as-rigid-as-possible (ARAP) energy. As this network is constructed for data with fixed point to point correspondences we cannot compare its performance on the unregistered testing set, but only use it for pre-registered data. Finally, we compare our results to those obtained with 3D-Coded [12], which models deformations using an auto-decoder with regularization using again an ARAP energy. In contrast to the auto-encoder network of [17], 3D-Coded utilizes a PointNet architecture as encoder to enable invariance to parameterization thereby allowing us to apply this method also to unregistered data. We train and validate all of the methods presented in this work with the same training and testing split of the DFAUST dataset as our method.

#### 3.1.1 Results:

A quantitative comparison for the latent code retrieval task is presented in Table 1: as one can see VariShaPE significantly outperforms Chamfer search and the VAE based method [17], while being comparable to 3D-Coded [12]. At the same time VariShaPE has an order of magnitudes lower computational cost than Chamfer search and 3D-coded (approximately 5.000 times faster) and a somewhat lower (but comparable) computational cost than the VAE based approach of [17]. In addition to these quantitative results, we present qualitative results in Figure 4; here we restrict the comparison to Chamfer search and 3D-Coded as we focus the presentation to the more challenging task of retrieving the latent code directly from unregistered and noisy scans. One can clearly see the superior performance of our method and 3D-Coded reflected in these qualitative results. In addition one can observe that our method preforms well even w.r.t. fine details such as the muscle structure on the core, whereas 3D-Coded seems to loose these finer details. Note, that these fine texture-like details are not accurately measured with in the quantitative measurements.

#### 3.1.2 Mesh Invariance of the VariShaPE Model:

Finally, we want to carefully explore the sensitivity of the proposed method under remeshing operations, where we compare our results to those of Chamfer search and 3D-Coded, which, similar to VariShaPE, operate on unregistered data and should be thus insensitive to these operations. Towards this objective, we picked 100 shapes from our testing set in DFAUST and created for each

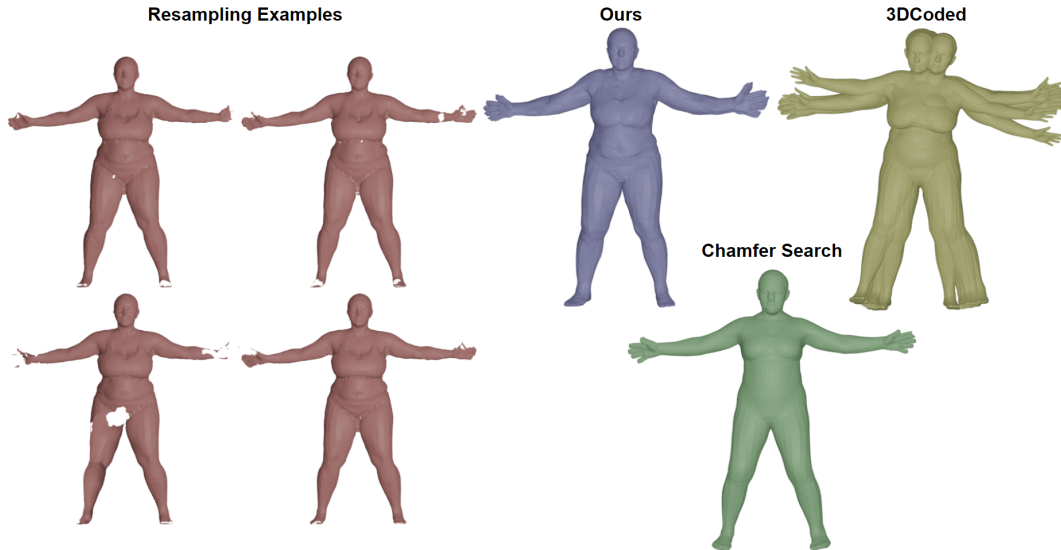


Figure 5: Qualitative results for mesh invariance: on the left, we display four examples of different meshes representing the same human body shape. On the right, we display the reconstructions of 100 such representations using our model (blue), Chamfer search (green), and 3D-coded (yellow). Our model displays invariance to these remeshing operations by producing consistent and accurate reconstructions of the set of meshes representing the same human body shape.

of these human body shapes 100 different representatives sampling vertices from the original mesh and applying meshing operations to the resulting point cloud, see Figure 5 for examples of different representations of the same human body shape. We then compared the obtained reconstruction for all 100 representatives, which should be near identical demonstrating the invariance of the different methods under these resampling operations. A qualitative comparison can be seen in Figure 5, whereas a quantitative analysis is presented in Table 2. As one can see, our method significantly outperforms the competing methods, where the performance issues of the other two methods are distinctive: the first method, 3D-Coded, struggles with producing a consistent reconstruction in the presence of mesh resamplings. The second method, Chamfer search, is more consistent but in general rather mediocre, i.e, there is a small variance in the Chamfer reconstructions but each of them has a relatively large error to the ground truth. In contrast our method produces consistent reconstructions with a small error to the ground truth, thereby demonstrating the robustness w.r.t. remeshing operations.

	Chamfer Search	3D Coded [13]	Ours
Mean Chamfer Error (mm)	5.7	4.0	<b>2.9</b>
Chamfer Error Variance (mm)	0.086	0.246	<b>0.074</b>
Varifold Error Variance	9.0e-4	2.5e-3	<b>5.7e-4</b>
Vertex Location Variance (mm)	1.25	4.79	<b>.038</b>

Table 2: Quantitative results for mesh invariance: We construct a set 100 classes of 100 reparameterizations of random meshes from our data set. We then present the mean of the intraclass standard deviations for the errors and vertex locations of the reconstructions.

## 3.2 Motion Interpolation and Extrapolation using MoGeN

### Experimental Setup:

Next we investigate the capabilities of our second model, MoGeN, to accurately learn the geometry of a latent space representation of human body motions. We report results for the latent space representation of motions for the base, gender-neutral SMPL model. We take  $N = 1500$  as dimension for the lifted latent space. The maps  $f, \pi$  are constructed as fully connected networks using ReLU activation functions and a combined  $2 \times 10^7$  trainable parameters.

### Comparison Methods:

To evaluate the performance of MoGeN we evaluate our approach against two competing state-of-the-art methods: first, we compare to linear interpolations in the pose parameter space of the SMPL model, which is a common approach in the SMPL community as linear interpolations correspond to joint rotations. This is a natural baseline to compare our model against and further allows us to visualize differences of the corresponding paths in latent space, c.f Figure 6 and Figure 7. Second, we provide a comparison to ARAPReg, the auto-decoder latent space construction of [17].

### Results:

In Table 3 one can observe that the proposed algorithm significantly outperforms the competing methods, which is also visualized in the qualitative examples in Figures 6 and 7. We note that the difference in the quantitative results seems significantly lower than the qualitative results suggest: the reason for this is that large parts of the body remain unmoved in these experiments and thus even the significantly worse results of the competing methods have a decent overlap in large regions of the human body, i.e., in those that do not significantly move.

Finally, we note that the computational times for all three methods are on a similar scale (in the order of 2 milliseconds for each of the methods), while the training time of our method is significantly lower than ARAPReg (12 hours as compared to two weeks).

	Interpolation			Extrapolation		
	Linear	ARAPReg [17]	MoGeN (Ours)	Linear	ARAPReg [17]	MoGeN (Ours)
Mean Vertex Error (mm)	1.26	1.03	<b>0.46</b>	1.42	1.27	<b>0.59</b>
Chamfer Error (mm)	0.70	0.66	<b>0.53</b>	0.85	0.82	<b>0.64</b>
Varifold Error	0.0073	0.0069	<b>0.0060</b>	0.0092	0.0088	<b>0.0071</b>
Timing For $10^3$ Sequences	1.6s	2.2s	1.9s	1.6s	2.2s	1.9s
Training Time	None	2w	12hrs	None	2w	12hrs

Table 3: Interpolation and extrapolation results for SMPL model: We compute the mean vertex distance and mean varifold error for the testing set of mini-sequences extracted from the DFAUST testing set.

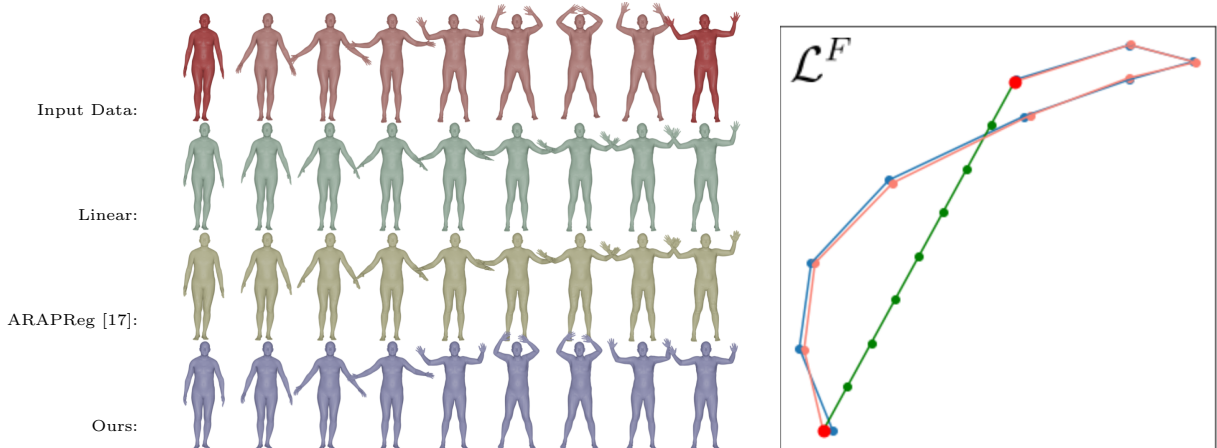


Figure 6: Qualitative comparison of MoGeN with linear interpolations in SMPL space and with ARAPReg paths. In red, we display a sequence of meshes from a human motion of the dataset with the boundary points highlighted. In green, we display the path which arises from linear interpolation between the boundary points in the latent space  $\mathcal{L}^F$  while the yellow sequence shows the results obtained with ARAPReg [17]. Finally, in blue, we display the path produced by the MoGeN interpolation model with the boundary points as inputs. On the right, we visualize these paths in a two-dimensional subspace of  $\mathcal{L}^F$ , with the same color coding (the ARAPReg path is not shown there as it involves a different latent space)

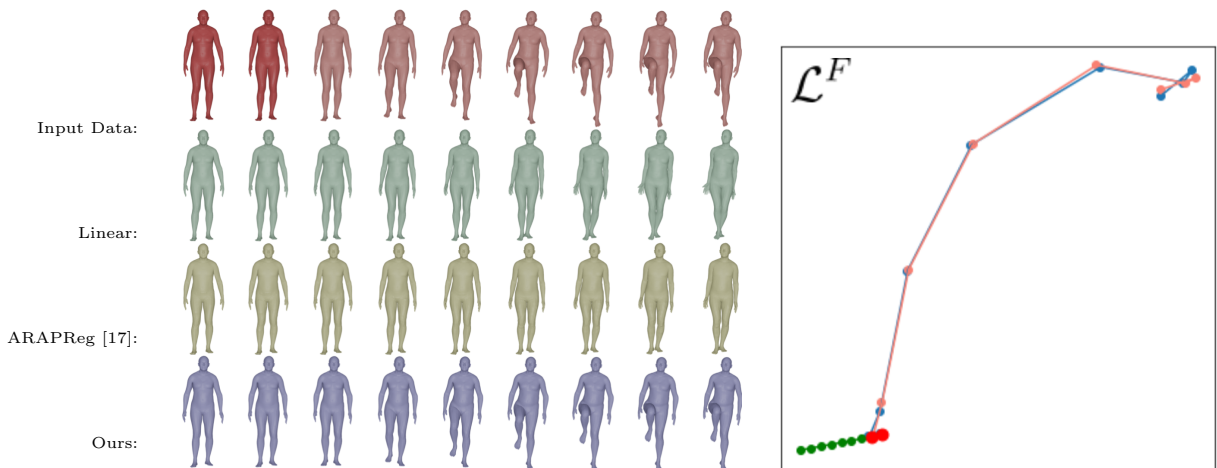


Figure 7: Qualitative comparison of MoGeN with linear extrapolation in SMPL space and based on the ARAPReg framework. In red, we display a body motion sequence extracted from data with the initial two points highlighted. In green is shown the path arising from linear extrapolation from the initial points in the latent space, and in yellow the path obtained from ARAPReg [17]. Finally, in blue, we display the path produced by the MoGeN extrapolation model with the boundary points as inputs. On the right plot, we visualize these paths in a two-dimensional subspace of  $\mathcal{L}^F$  using the same color coding.

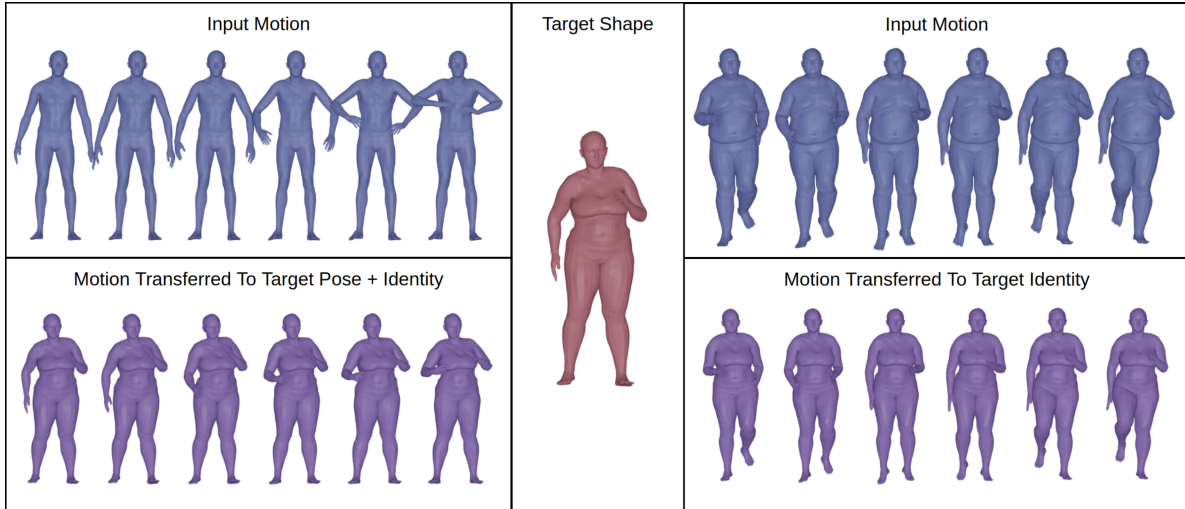


Figure 8: Examples of Motion Transfer: On the right we display the transfer of a motion from data (blue) to the identity of a different target shape (red). Using the VariShaPE model we obtain latent codes for the target motion and shape. We then combine the pose parameters of the motion with the identity parameters of the target to produce an transferred motion (purple). On the left we display the transfer of body motion from data (blue) onto the *pose and identity* of the target shape (red). Using MoGeN, we obtain lifted pose parameters for the sequence and target shape and apply a simple translation in the lifted space. We map the resulting path back to to the latent space and combine the transferred pose parameters with the target identity parameters producing the transferred motion (purple).

## 4 Applications to Motion Transfer, Generative Modeling and Interpolation between 4D-data.

In this final section, we complement the results of the previous section by presenting a few different possible applications of the proposed methodology.

### 4.1 Motion transfer

A first example of application is real-time motion transfer, i.e., we consider the problem of transferring a motion from one human body shape to another, cf. Figure 8 for two different examples. Combining VariShaPE and MoGeN immediately leads to a natural and efficient algorithm for that purpose: given a motion sequence (represented by a series of meshes) and a target shape, we map all those meshes in the SMPL latent space  $\mathcal{L}^F$  using the VariShaPE model. This leads to the motion being represented as a path in latent space and the target shape as a point. Subsequently we employ MoGeN to accurately transport the corresponding path of latent codes to the latent code of the target; namely, the path and the point are lifted to the auxiliary latent space of MoGeN, which is equipped with a simple Euclidean geometry, and thus one can apply a simple translation of the path in this space.

### 4.2 Generative modeling in the space of human body shapes:

Next, we demonstrate how one can combine MoGeN and VariShaPE to obtain a generative model for human bodies based on estimating an empirical distribution from observed training data. In



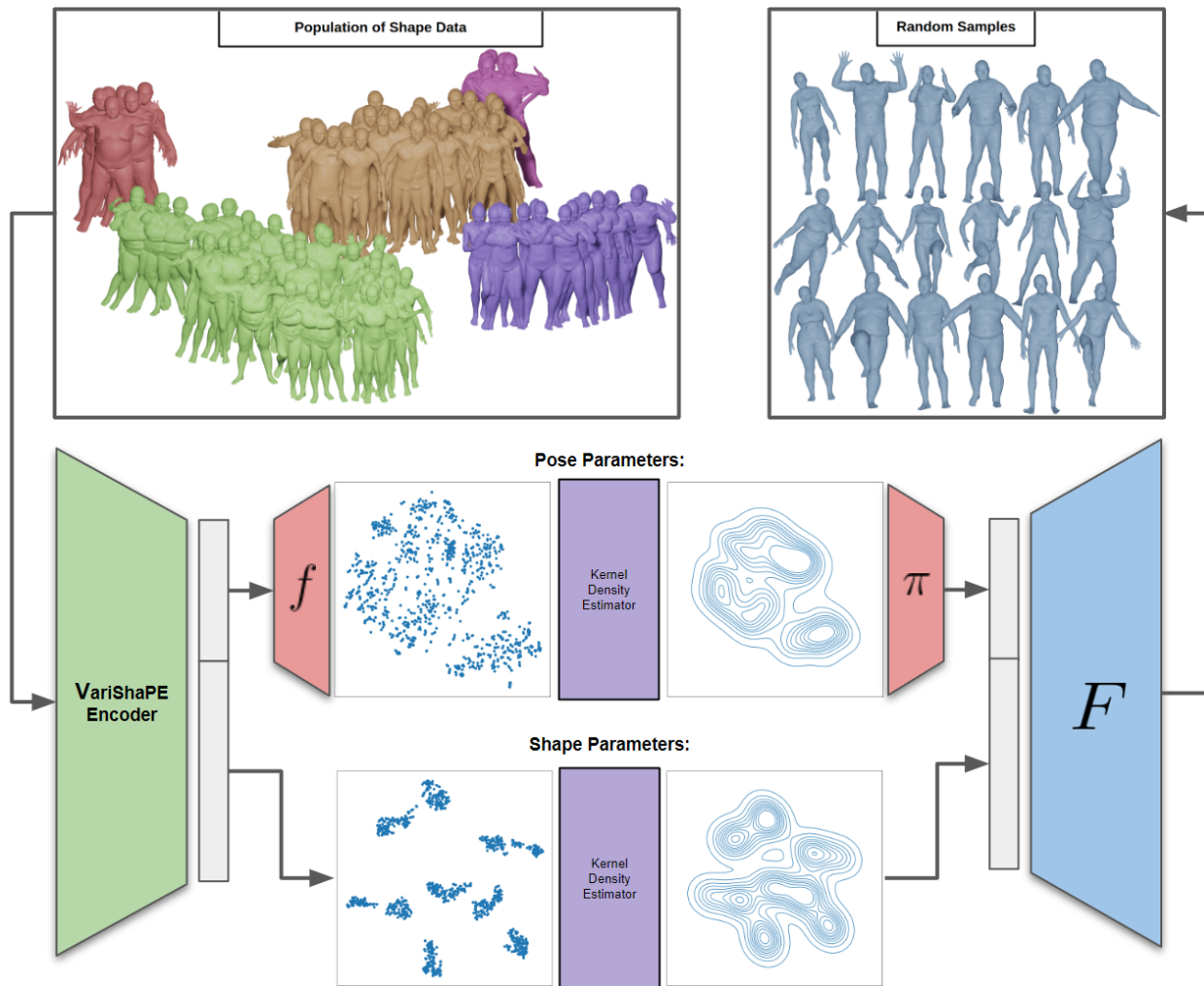


Figure 9: Here we describe the pipeline for a generative model based on our networks based on an empirical distribution of human bodies. First, we extract the pose and identity parameters of a dataset of human bodies using the VariShaPE model. We apply MoGeN to the distribution of pose parameters and fit a kernel density estimator (KDE) in the lifted space. To generate a new pose we sample a code from this KDE and map it back to the latent space. We combine this with an identity code sampled from a KDE fit to the distribution of identity parameters to generate a random shape.



Figure 10: Interpolations between 4D data: we display two interpolation examples between 4D data using our models. The top and bottom rows correspond to two 4D motion sequences with the middle rows corresponding to the interpolation based on our approach. The example on the right demonstrates the ability of the algorithm to interpolate between motions that are performed at different speeds: we show the interpolation between the first half of a sequence to the full sequence, i.e., the second sequence performs the motion in half the time. Instead of blending the motion at each fixed time our algorithm correctly extends the length of the motion in the interpolation. The highlighted shape shows the moving endpoint of the first sequence.

Figure 9, we show 18 random samples from an empirical distribution constructed using 30,000 scans. Note, that this procedure is only feasible due to the light speed encoding capabilities for raw scans via VariShaPE: for our experiment the encoding of the whole population of unregistered training scans took less than one minute. Note that, comparatively, the construction of a similar empirical distribution (i.e., the encoding of the 30,000 scans) using 3D-Coded would require over 2 days. Rather than directly applying kernel density estimator in the SMPL space, we followed the same procedure as in the motion transfer application and first lifted the data into the auxiliary latent space of MoGeN. The linear geometry of that space allows us to use kernel density estimation in a more principled way while still capturing the non-linear nature of the space of human body motion, cf. Figure 9 for a schematic of this procedure.

### 4.3 Interpolation and extrapolation of 4D-data

As a third example, we show how our frameworks can be combined to lead to an algorithm for 4D-data interpolation (and extrapolation), i.e., we aim to interpolate (extrapolate, resp.) between two motion sequences  $q_1(t)$  and  $q_2(t)$ . A simple algorithm for achieving this goal would consist of interpolating for each fixed time  $t_0$  in the motion sequences between their corresponding latent codes. This can lead, however, to sub-optimal results as humans perform motions at varying speed and thus  $q_0(t_0)$  might not correspond to  $q_1(t_0)$  but rather to a different time point  $q_1(t_1)$ . To address this challenge we resort to MoGeN, which maps motion sequences to straight lines in the lifted latent space. This allows to reduce the 4D-interpolation problem to the task of averaging lines in  $\mathbb{R}^N$ . We present two examples of this procedure in Figure 10, where the time independence

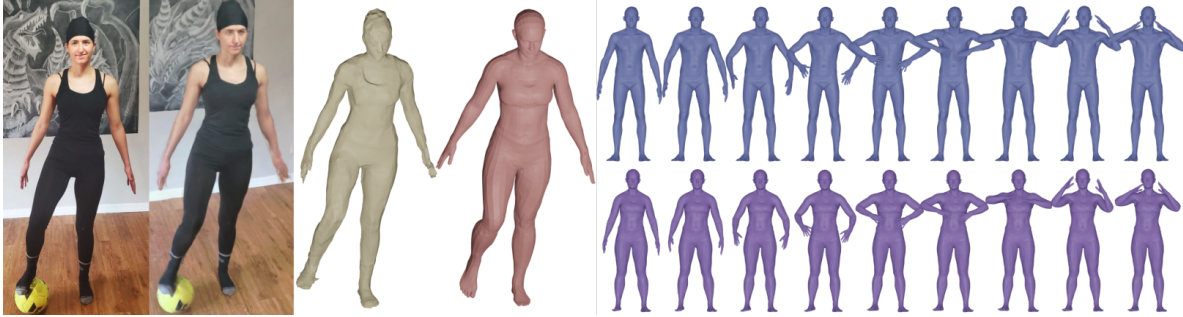


Figure 11: An example using Neural Radiance Field reconstruction from a body shape video scanned: On the left we show the retrieval of the latent code representation of a surface reconstructed from a Neural Radiance Field representation of the subject. On the right, we display a motion sequence on the top row and the transferred motion sequence with the selected identity.

of the 4D-interpolation algorithm is highlighted by the example on the right.

#### 4.4 Representation of scans obtained from neural radiance field reconstruction

An important aspect of the proposed methods is the use of mesh invariant feature representations as inputs of the neural networks which a priori allows them to be applied to raw unregistered and noisy meshes with limited pre-processing needed beyond usual rigid alignment. This includes meshes obtained from different scanning modalities as the result of Figure 11 shows with a surface obtained from neural radiance field reconstruction that the authors directly acquired using their cellphone camera. One shortcoming this result points to, however, is the oversimplification of the body shape for subjects too different from those that can be represented in the latent space. We should note that this is primarily a limitation of the latent space used for body shape representation. As the generic framework of this paper is not tied to a specific choice of latent representation, we hope to address such issues in future iterations of this work.

## Acknowledgements

N.C and E.H were supported by the National Science Foundation, under the grants DMS-2438562 and DMS-2402555. M. B. was supported by the National Science Foundation, under the grant DMS-2324962, and by the Binational Science Foundation (BSF).

## A Ablation Study using a different Latent space models

### A.1 The VariShape model using the elastic shape analysis latent space of [15]

In Section 4, we reported the performance of VariShaPE using SMPL [19] as the latent model  $F$  and the model proposed by [15] as the feature map  $G$ . In Table 4, we further explore the performance of the VariShaPE for alternate combinations of  $F$  and  $G$ . These combinations allow us to examine the robustness and adaptability of the VariShaPE framework when employing different underlying latent space and feature models. The VariShaPE model achieves consistently strong performance across these variations, demonstrating its effectiveness regardless of the specific models used for  $F$  and  $G$ . Nonetheless, the combination highlighted in the main paper yields slightly superior results, suggesting it is the optimal configuration among those tested.

	F: BaRe[15]		G: BaRe[15]			F: SMPL[19]		G: SMPL[19]	
	Registered	Unregistered	Registered	Unregistered		Registered	Unregistered	Registered	Unregistered
Mean Error	2.1mm	NA			Mean Error	2.2mm	NA		
Varifold Error	0.034	0.037			Varifold Error	0.037	0.041		
Chamfer Error	2.5mm	3.0mm			Chamfer Error	2.8mm	3.4mm		

Table 4: Ablation study for various choices of  $F$  and  $G$  in VariShaPE. In the left table, we present results with  $F$  and  $G$  chosen to be the latent space model of [15]. The right table contains the results where  $F$  and  $G$  are chosen to be the latent space model of SMPL [19].

## A.2 The MoGen model for the elastic shape analysis latent space of [15]

Section 4 also reports and discusses the results of the MoGen model applied to the SMPL latent space [19]. To further investigate the model’s versatility, Table 5 presents the results of MoGen applied to the latent space defined by [15]. These results indicate that it performs comparably well within this alternative latent space. The findings suggest that the MoGen model maintains

	Interpolation		Extrapolation	
	Linear	MoGen	Linear	MoGen
Mean Error	0.61mm	0.56mm	1.73mm	0.61mm
Varifold	0.0072	0.0066	0.0078	0.0069

Table 5: Interpolation and Extrapolation Results for the model of [15]: We present the mean vertex error and mean varifold error of paths in the latent space of [15] produced by the MoGen model. We report the results for the testing set of mini-sequences extracted from the DFAUST testing set.

its effectiveness regardless of the choice of latent space, performing similarly to its results with the SMPL model.

## B Ablation Study on the Choice of Loss Function in VariShaPE

Finally, we conduct an ablation study on the choice of loss function used in training of the VariShaPE model. We present the results for the model trained with these losses evaluated on an unseen testing set. While the combination of mean vertex error and varifold error yields marginally

	Registered			Unregistered		
	Mean Vertex	Dist.	Varifold	Chamfer	Varifold	Chamfer
Mean Vertex	2.1mm		0.035	2.5mm	0.036	<b>2.9mm</b>
Chamfer	2.0mm		0.030	2.0mm	0.035	3.3mm
Varifold	2.4mm		0.028	2.7mm	0.033	3.6mm
Varifold + Mean Vertex	<b>1.8mm</b>		<b>0.026</b>	<b>2.2mm</b>	<b>0.033</b>	3.4mm
Varifold + Chamfer	2.1mm		0.030	2.2mm	0.036	3.0mm

Table 6: Ablation Study for training the VariShaPE model with different choices of loss function.

superior results, we focus on the model trained exclusively with mean vertex error. This decision is motivated by practical considerations, as the mean vertex error-only model achieves nearly equivalent performance while reducing training time by approximately 4 hours.

## References

- [1] B. B. Amor, S. Arguillère, and L. Shao. ResNet-LDDMM: advancing the LDDMM framework using deep residual networks. *IEEE Transactions on Pattern Analysis and Machine Intelligence*, 45(3):3707–3720, 2022.

- [2] D. Anguelov, P. Srinivasan, D. Koller, S. Thrun, J. Rodgers, and J. Davis. SCAPE: Shape Completion and Animation of People. In *ACM SIGGRAPH 2005 Papers*, pages 408–416. 2005.
- [3] M. Atzmon, D. Novotny, A. Vedaldi, and Y. Lipman. Augmenting Implicit Neural Shape Representations with Explicit Deformation Fields. *arXiv preprint arXiv:2108.08931*, 2021.
- [4] V. Blanz and T. Vetter. A Morphable Model for the Synthesis of 3D Faces. In *Annual Conf. on Computer Graphics and Interactive Techniques (SIGGRAPH)*, pages 187–194, 1999.
- [5] F. Bogo, J. Romero, G. Pons-Moll, and M. J. Black. Dynamic FAUST: Registering Human Bodies in Motion. In *IEEE Conf. on Computer Vision and Pattern Recognition (CVPR)*, July 2017.
- [6] R. Q. Charles, H. Su, M. Kaichun, and L. J. Guibas. PointNet: Deep Learning on Point Sets for 3D Classification and Segmentation. In *2017 IEEE Conference on Computer Vision and Pattern Recognition (CVPR)*, page 77–85. IEEE, Jul 2017.
- [7] N. Charon, B. Charlier, J. Glaunès, P. Gori, and P. Roussillon. Fidelity Metrics between Curves and Surfaces: Currents, Varifolds, and Normal Cycles. In *Riemannian geometric statistics in medical image analysis*, pages 441–477. Elsevier, 2020.
- [8] L. Cosmo, A. Norelli, O. Halimi, R. Kimmel, and E. Rodolà. Limp: Learning latent shape representations with metric preservation priors. In *Computer Vision–ECCV 2020: 16th European Conference, Glasgow, UK, August 23–28, 2020, Proceedings, Part III 16*, pages 19–35. Springer, 2020.
- [9] H. Fan, H. Su, and L. J. Guibas. A Point Set Generation Network for 3D Object Reconstruction from a Single Image. In *Proceedings of the IEEE conference on computer vision and pattern recognition*, pages 605–613, 2017.
- [10] O. Freifeld and M. J. Black. Lie Bodies: A Manifold Representation of 3D Human Shape. *ECCV (1)*, 7572:1–14, 2012.
- [11] A. Gretton, K. Borgwardt, M. Rasch, B. Schölkopf, and A. Smola. A kernel method for the two-sample-problem. *Advances in neural information processing systems*, 19, 2006.
- [12] T. Groueix, M. Fisher, V. G. Kim, B. Russell, and M. Aubry. 3d-coded : 3d correspondences by deep deformation. In *ECCV*, 2018.
- [13] T. Groueix, M. Fisher, V. G. Kim, B. C. Russell, and M. Aubry. 3d-coded: 3d correspondences by deep deformation. In *Proceedings of the European Conference on Computer Vision (ECCV)*, pages 230–246, 2018.
- [14] E. Hartman and E. Pierson. VariGrad: A Novel Feature Vector Architecture for Geometric Deep Learning on Unregistered Data. In *Eurographics Workshop on 3D Object Retrieval*, 2023.
- [15] E. Hartman, E. Pierson, M. Bauer, N. Charon, and M. Daoudi. BaRe-ESA: A Riemannian Framework for Unregistered Human Body Shapes. In *Proceedings of the IEEE/CVF International Conference on Computer Vision (ICCV)*, pages 14181–14191, October 2023.
- [16] N. Hasler, C. Stoll, M. Sunkel, B. Rosenhahn, and H.-P. Seidel. A Statistical Model of Human Pose and Body Shape. In *Computer graphics forum*, volume 28, pages 337–346. Wiley Online Library, 2009.

- [17] Q. Huang, X. Huang, B. Sun, Z. Zhang, J. Jiang, and C. Bajaj. Arapreg: An as-rigid-as possible regularization loss for learning deformable shape generators. In *Proceedings of the IEEE/CVF International Conference on Computer Vision*, pages 5815–5825, 2021.
- [18] I. Kaltenmark, B. Charlier, and N. Charon. A general framework for curve and surface comparison and registration with oriented varifolds. In *Proceedings of the IEEE Conference on Computer Vision and Pattern Recognition*, pages 3346–3355, 2017.
- [19] M. Loper, N. Mahmood, J. Romero, G. Pons-Moll, and M. J. Black. SMPL: A skinned multi-person linear model. *ACM Trans. Graphics (Proc. SIGGRAPH Asia)*, 34(6):248:1–248:16, Oct. 2015.
- [20] L. Mi, T. He, C. F. Park, H. Wang, Y. Wang, and N. Shavit. Revisiting latent-space interpolation via a quantitative evaluation framework. *arXiv preprint arXiv:2110.06421*, 2021.
- [21] M. Y. Michelis and Q. Becker. On linear interpolation in the latent space of deep generative models. In *ICLR 2021 Workshop on Geometrical and Topological Representation Learning*, 2021.
- [22] S. Muralikrishnan, S. Chaudhuri, N. Aigerman, V. G. Kim, M. Fisher, and N. J. Mitra. GLASS: geometric latent augmentation for shape spaces. In *Proceedings IEEE Conf. on Computer Vision and Pattern Recognition (CVPR)*, June 2022.
- [23] S. Muralikrishnan, C.-H. P. Huang, D. Ceylan, and N. J. Mitra. Bliss: Bootstrapped linear shape space. *arXiv preprint arXiv:2309.01765*, 2023.
- [24] A. A. A. Osman, T. Bolkart, and M. J. Black. STAR: A Sparse Trained Articulated Human Body Regressor. In *European Conference on Computer Vision (ECCV)*, pages 598–613, 2020.
- [25] M. Ovsjanikov, M. Ben-Chen, J. Solomon, A. Butscher, and L. Guibas. Functional Maps: a flexible representation of maps between shapes. *ACM Transactions on Graphics (TOG)*, 31(4):1–11, 2012.
- [26] G. Pavlakos, V. Choutas, N. Ghorbani, T. Bolkart, A. A. A. Osman, D. Tzionas, and M. J. Black. Expressive body capture: 3D hands, face, and body from a single image. In *Proceedings IEEE Conf. on Computer Vision and Pattern Recognition (CVPR)*, pages 10975–10985, 2019.
- [27] E. Pierson, M. Daoudi, and S. Arguillère. 3D Shape Sequence of Human Comparison and Classification Using Current and Varifolds. In S. Avidan, G. Brostow, M. Cissé, G. M. Farinella, and T. Hassner, editors, *Computer Vision – ECCV 2022*, pages 523–539, Cham, 2022. Springer Nature Switzerland.
- [28] E. Pierson, M. Daoudi, and A.-B. Tumpach. A riemannian framework for analysis of human body surface. In *Proceedings of the IEEE/CVF Winter Conference on Applications of Computer Vision (WACV)*, pages 2991–3000, January 2022.
- [29] L. Pishchulin, S. Wuhrer, T. Helten, C. Theobalt, and B. Schiele. Building Statistical Shape Spaces for 3D Human Modeling. *Pattern Recognition*, 67:276–286, 2017.
- [30] Ł. Struski, M. Sadowski, T. Danel, J. Tabor, and I. T. Podolak. Feature-based interpolation and geodesics in the latent spaces of generative models. *IEEE Transactions on Neural Networks and Learning Systems*, 2023.

- [31] G. Tiwari, D. Antić, J. E. Lenssen, N. Sarafianos, T. Tung, and G. Pons-Moll. Pose-ndf: Modeling human pose manifolds with neural distance fields. In S. Avidan, G. Brostow, M. Cissé, G. M. Farinella, and T. Hassner, editors, *Computer Vision – ECCV 2022*, pages 572–589, Cham, 2022. Springer Nature Switzerland.
- [32] Wang, Yue and Sun, Yongbin and Liu, Ziwei and Sarma, Sanjay E and Bronstein, Michael M and Solomon, Justin M. Dynamic graph CNN for learning on point clouds. *ACM Transactions On Graphics (TOG)*, 38(5):1–12, 2019.